

Propagating slow sausage waves in a sunspot observed by the New Vacuum Solar Telescope

Song Feng^{1,2,4}, Zheng Deng¹, Ding Yuan^{3*}, Zhi Xu⁴ and Xiao Yang²

¹ Faculty of Information Engineering and Automation, Kunming University of Science and Technology, Kunming 650500, China; feng.song@kust.edu.cn

² Key Laboratory of Solar Activity, National Astronomical Observatories, Chinese Academy of Sciences, Beijing 100101, China

³ Institute of Space Science and Applied Technology, Harbin Institute of Technology, Shenzhen 518055, China; yuanding@hit.edu.cn

⁴ Yunnan Observatories, Chinese Academy of Sciences, Kunming 650011, China

Received 2020 January 16; accepted 2020 February 8

Abstract A sunspot is an ideal waveguide for a variety of magnetohydrodynamic waves, which carry a significant amount of energy to the upper atmosphere and could be used as a tool to probe the magnetic and thermal structure of a sunspot. In this study, we used the New Vacuum Solar Telescope and took high-resolution image sequences simultaneously in both TiO ($7058\pm 10\text{ \AA}$) and H $_{\alpha}$ ($6562\pm 2.5\text{ \AA}$) bandpasses. We extracted the area and total emission intensity variations of sunspot umbra and analyzed the signals with synchrosqueezing transform. We found that the area and emission intensity varied with both three and five minute periodicity. Moreover, the area and intensity oscillated in phase with each other, this fact hold in both TiO and H $_{\alpha}$ data. We interpret this oscillatory signal as a propagating slow sausage wave. The propagation speed is estimated at about 8 km s^{-1} . We infer that this sunspot's umbra could have temperature as low as 2800–3500 K.

Key words: Sun: sunspot — Sun: oscillations — magnetohydrodynamics (MHD) — methods: data analysis

1 INTRODUCTION

The solar atmosphere is a highly dynamic and magnetized plasma. Many solar activities and phenomena are observed in the solar atmosphere. Magnetohydrodynamic (MHD) waves are commonly found in the magnetized plasma and can be observed in a variety of magnetic structures, such as sunspots (Jess et al. 2013; Su et al. 2016; Yuan & Walsh 2016; Wang et al. 2020; Bai et al. 2013), pores (Dorotovic et al. 2014; Grant et al. 2015; Moreels et al. 2015; Freij et al. 2016), and coronal loops (Inglis et al. 2009; Nakariakov et al. 2012; Yuan et al. 2015; Tian et al. 2016).

MHD waves are usually modified by a magnetic field. They can perturb the plasma density and magnetic field, therefore, they are further classified as Alfvén waves (Goossens et al. 2013; Bai et al. 2014), slow and fast magnetoacoustic waves (Inglis et al. 2009;

Vasheghani Farahani et al. 2014; Li et al. 2014; Yu et al. 2016; Keys et al. 2018; Chen et al. 2015; Chen et al. 2018). Linear Alfvén waves can propagate along magnetic fields without perturbing the plasma pressure and density, whereas slow and fast magnetoacoustic waves are compressible waves associated with perturbations in the plasma and magnetic pressure.

Sausage modes are compressible magnetoacoustic waves that are featured by axially symmetric perturbations in magnetic flux tubes. This attracts interest because of their potential role in chromospheric and coronal heating. They can be classified into slow and fast modes based on their axial phase speeds (Edwin & Roberts 1983). Another main difference between two sausage-mode forms is the phase relationship between their cross-section area and intensity variations. In case of fast sausage mode, these two values oscillate out-of phase, whereas they are in phase for slow sausage modes (Moreels et al. 2013; Dorotovic et al. 2014). Investigating sausage waves and their propagation in the lower solar atmosphere is important for understand-

* Corresponding author

ing the wave energy propagation and release in the entire solar atmosphere.

In the coronal context, it has been a common practice to invoke sausage modes to account for quasi-periodic pulsations in solar flare light curves with quasi-periods of the order of seconds (for recent reviews, see e.g., Nakariakov & Melnikov 2009 and McLaughlin et al. 2018). However, it remains to show a definitive piece of observational evidence demonstrating the existence of sausage waves in coronal structures (see e.g., sect. 4 in Shi et al. 2019).

Recently, due to high spatial and temporal observations provided by ground-based instruments, the direct evidence of sausage modes in the lower solar atmosphere have been reported (Dorotovic et al. 2014; Grant et al. 2015; Freij et al. 2016). Dorotovic et al. (2014) investigated the perturbation relations between cross-sectional areas and total intensities in a sunspot and two pores, and they detected the sausage modes with periods from 4 to 65 minutes. By analyzing the ratio between different periodic values, they further revealed that the oscillation modes can be considered as standing waves. Multiple-channel observations are employed to investigate upward propagating sausage waves from the lower photosphere to the upper photosphere/lower chromosphere (Grant et al. 2015). According to the energies carried by sausage modes, the authors found that the wave energies decrease substantially with heights and inferred that the energies could be released into the surrounding chromospheric plasma. Freij et al. (2016) inferred that the sausage modes detected in two photospheric pores are standing harmonics with strong reflections at the transition region. Keys et al. (2018) present evidence of surface and body modes in photospheric pores supporting sausage waves at the frequency ranging between 2 and 12 mHz.

The purpose of this study is to analyze the perturbations in both areas and intensities within a nearly circular sunspot umbra observed in two different passbands, thereby looking for evidence of sausage waves propagating from photospheric to chromospheric heights. This paper is structured as follows: Section 2 describes our observations and data reduction. Our results are presented in Section 3. Finally, Section 4 discusses and concludes this study.

2 OBSERVATIONS AND DATA REDUCTION

In this study, we focus on active region NOAA 11809, its heliocentric co-ordinates were ($95''$, $20''$) on 2013 August 6. Two co-spatial high-resolution image sequences were acquired by the New Vacuum Solar Telescope (NVST; Liu et al. 2014). The H_α ($6562.8 \pm 0.25 \text{ \AA}$) and TiO ($7058 \pm 10 \text{ \AA}$) channels were used to capture the chromospheric and photospheric images between 01:32 and 02:26 UT. The sampling interval was 25 s and 12 s for TiO

and H_α images, respectively. Each pixel in TiO images corresponded to $0.041''$ on the Sun; whereas in H_α images a pixel has an angular width of $0.165''$. Each sequence was co-aligned with sub-pixel accuracy with a user-defined registration algorithm (Feng et al. 2012). The TiO images were aligned with the H_α images after scaling and rotation. The formation height of the TiO channel is located at the lower part of the photosphere, and H_α at the upper part of the chromosphere.

Figure 1 shows the field-of-view provided by the TiO and H_α channels of NVST. The selected sunspot was close to the disk center and its shape was a nearly circular. We could consider this sunspot as a magnetic waveguide filled with stratified solar atmosphere. Therefore, this sunspot is an ideal model to investigate the periodic oscillations between area and intensity variations.

The area of sunspot umbra was detected by a thresholding method. To remove the effect of interference of strong penumbra emission, we used a boxcar with 25×25 pixels for the TiO data and 19×19 pixels for the H_α data to smooth the contours. Figure 1(a) and (b) shows detection of the area of the umbra. The emission intensity was summed up within the contour in each image and were normalized by the average intensity sampled at quiet sun region (red box in Fig. 1). This step ensures that the effect of atmospheric seeing was removed. Figure 2 shows the variation of the areas and normalized intensities measured in both TiO and H_α data. Here, the global trend of each time-vary curve was removed by 12 minute moving average to highlight the oscillation signatures.

Although the atmosphere seeing effect is removed by normalization as stated in the previous paragraph, we also further cross-validate the signal with space-borne instrument, the Atmospheric Imaging Assembly (AIA) onboard the Solar Dynamic Observatory (SDO). Consequently, we extracted the umbra area and emission intensity with 1700 \AA data. The results are presented in the Appendix (see Fig. A.1). We obtained very similar result with space-borne instrument, but the noise level is stronger than the NVST high-resolution data, so we only present the analysis with NVST channels thereafter.

The temporal variations of umbral area and total intensity were analyzed by synchrosqueezing transform (SST; Daubechies et al. 2011). SST is a novel time-frequency (TF) analysis method that precisely not only represent the power spectra of an oscillation signal, but also extract the intrinsic modes of the signal like empirical mode decomposition (Huang et al. 1998) but even higher accuracy (Daubechies et al. 2011). It is a derivation of continuous wavelet transform (CWT) empowered by a spectral reassignment algorithm that compensates the spreading inherent from CWT. The reassignment algorithm uses the phase information of CWT and concentrates on the spectral ener-

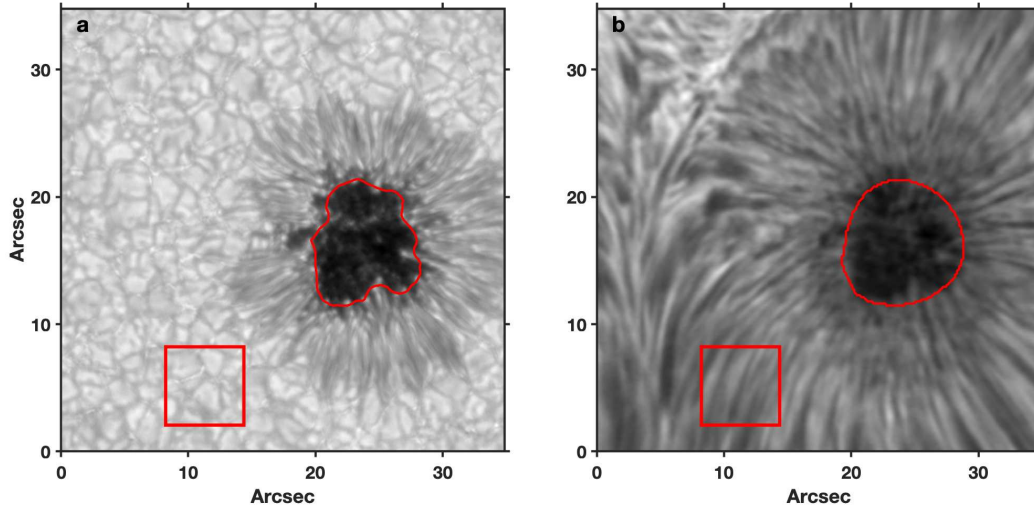


Fig. 1 Two images observed by the NVST instrument in the TiO (panel a) and H_{α} (panel b) channels at 01:32:29 UT 2013 August 6. Two *red contours* indicate the umbral edge identified, respectively. The two *boxes* mark the quiet regions that were used to normalize the intensities in the TiO and H_{α} images, respectively. This step ensures that the disturbance introduced by atmosphere of the Earth is removed.

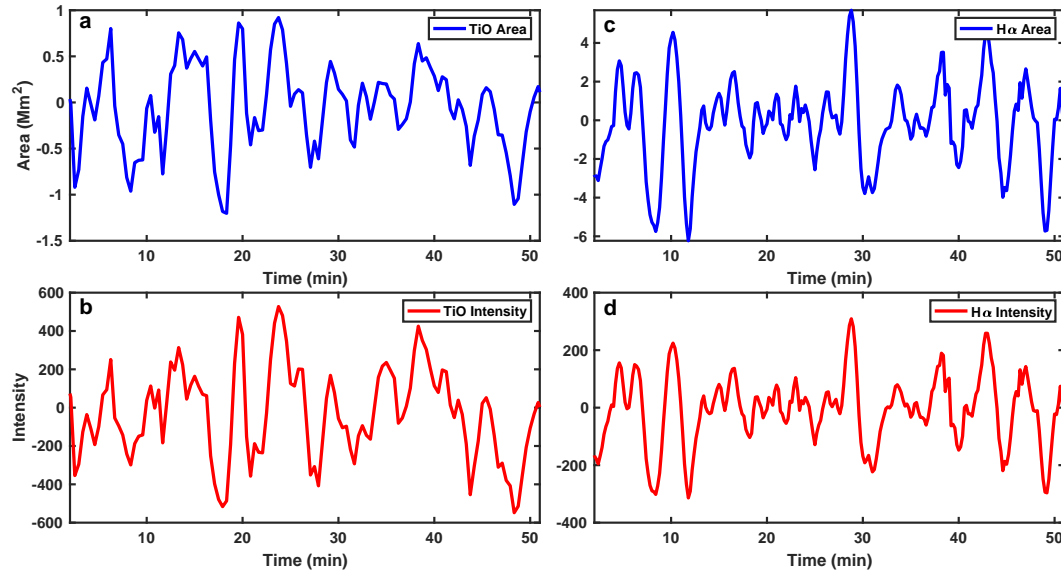


Fig. 2 Variations of the umbral areas (a) and intensities (b) obtained from the TiO data set. Panels (c) and (d) are the counterparts obtained in the H_{α} data set.

gy only along the frequency direction, therefore, it sharpens the wavelet spectrum, and in the meanwhile preserves the time resolution of the signal. Because SST concentrates on oscillatory modes into a narrow region in the TF plane and the energy concentration processing is invertible, this allows us to isolate and extract the energy ridge. In the TF plane, the local maxima are defined as the energy ridge, which indicates the frequency distributions of an intrinsic mode. SST uses a penalized forward-backward greedy algorithm to extract the energy ridges (Daubechies et al. 2011). This algorithm optionally constrains jumps in frequency with a penalty that is proportional to the square of

the distance between frequency bins. With this approach, the transform not only provides a perfect inversion, but also gives a stable the reconstruction. To non-stationary signals, SST not only provides spectral representation but also reconstructs its intrinsic modes as done in empirical mode decomposition. The phase relation between area and intensity oscillations is calculated to constrain the MHD wave mode, therefore, their intrinsic modes were reconstructed to calculate the oscillation phase, see Figures 3 and 4. The spectra and the modes of the SDO data are presented in the Appendix (see Fig. A.2).

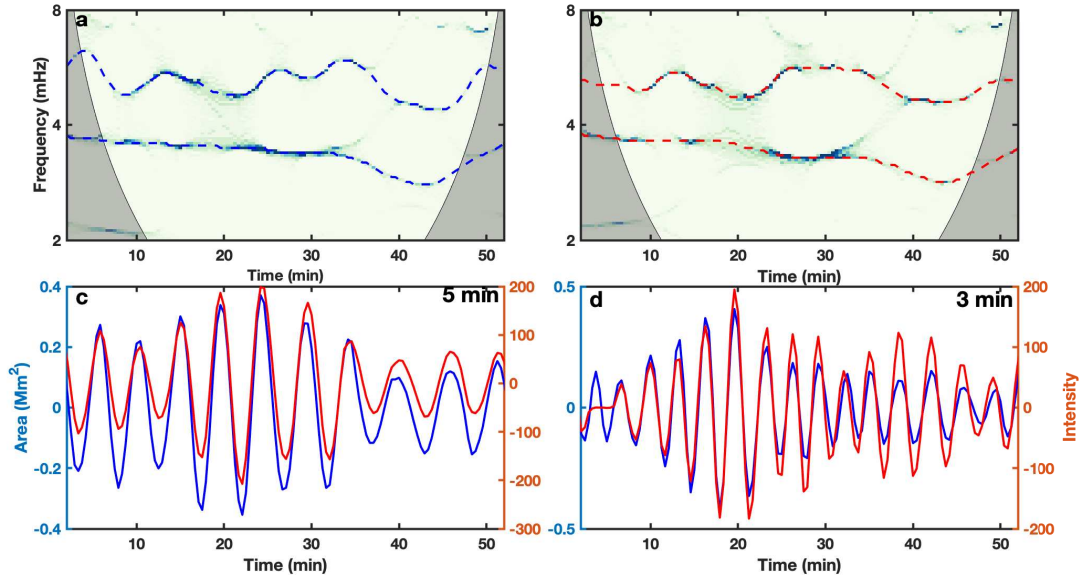


Fig. 3 SST power spectra of the area (a) and intensity (b) perturbations as plotted in Figs. 2(a) and 2(b). The *thin dashed lines* indicate the positions of the energy ridges that represent the local maxima. Panels (d) and (c) are reconstructed signal in the three and five minute bands, respectively. The area is plotted with *blue lines*, and the intensity with *red lines*. This analysis was conducted with the TiO data set.

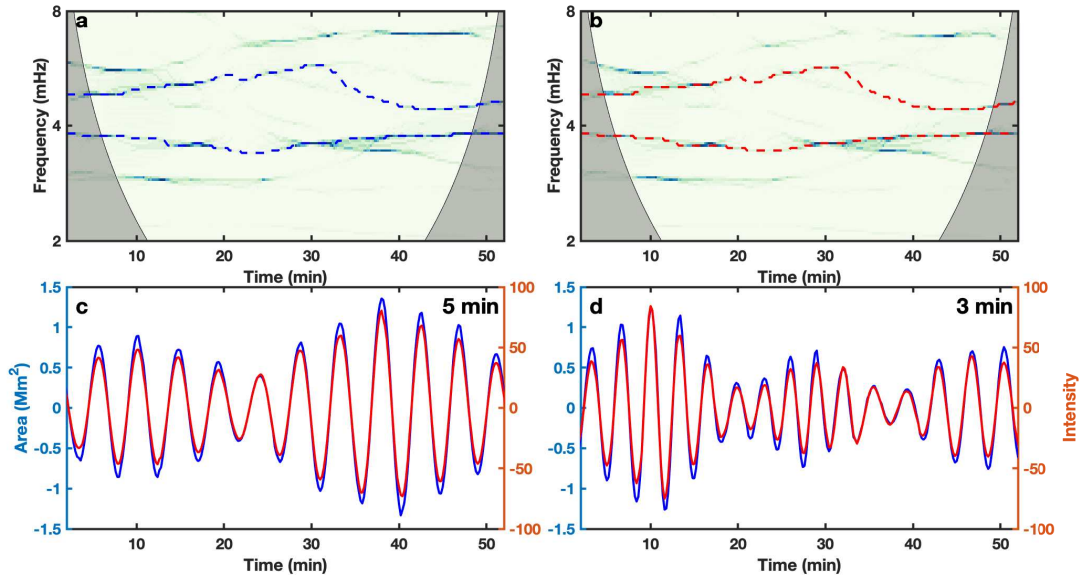


Fig. 4 Same as Fig. 3 but with the H_{α} data set.

Table 1 Mean and Standard Deviation of Three and Five Periods

		TiO	H_{α}	Lag Time
Five minute band	Area	4.94 ± 0.39	4.55 ± 0.18	180 ± 12 s
	Intensity	4.95 ± 0.36	4.53 ± 0.15	
Three minute band	Area	2.89 ± 0.39	3.36 ± 0.26	168 ± 12 s
	Intensity	3.21 ± 0.23	3.20 ± 0.25	

3 RESULT

The NVST TiO channel records the dynamics at the photospheric height, we use this data set to analysis the umbra oscillation therein. Figures 3(a) and (b) show power spec-

tra of the umbral area and intensity perturbations plotted in Figure 2. We could see that significant oscillation power were detected at 3–4 mHz (five minute bandpass) and 5–6 mHz (three minute bandpass). The SST power spectra of

both the area variation (Fig. 3(a)) and intensity (Fig. 3(b)) were very similar to each other.

We construct the narrowband oscillatory signal of both umbra area and emission intensity at three (Fig. 3(d)) and five minute bandpass (Fig. 3(c)), the reconstructed signal could reveal the phase relationship between the area and intensity variation. We can see the five minute oscillation where the umbra area oscillated in phase with the emission intensity. This is a signal of propagating slow mode wave, see the simulation in Yuan et al. (2016).

Similar analysis was performed to the NVST H_α channel, which observe the dynamics at the chromosphere of the sunspot. We detect similar oscillatory signals and phase relationship in this channel. The detected periods in both area and intensity variations for NVST channels are summarized in Table 1.

To study the propagation feature of the umbral wave between two layers observed by the NVST H_α and TiO channels, we combined these two channels and measured the lag time between them. The cross-correlation was calculated between the area variation measured at the TiO channel and that in the H_α . The lag time for the five minute band is about 168 ± 12 s; whereas the counterpart in the three minute band was about 180 ± 12 s.

4 CONCLUSIONS AND DISCUSSIONS

In this study, we used the NVST multi-channel observations and analysed the oscillatory signals in sunspot AR 11809. This sunspot was a unipolar sunspot, which has an ideal magnetic and thermal structure and could act as an effective waveguide for MHD waves. The area and intensity variations of this sunspot were extracted in both the TiO and H_α channels.

In the area and intensity variations of the TiO channel, we detected two oscillatory signals at three minute and five minute bands. We found that at both bands, the intensity variation oscillated in phase with the area variation. This is the feature of a propagating longitudinal wave (Yuan et al. 2016). Similar results were found in the H_α channel.

If we combine two channels at TiO and H_α , which record the dynamics at the photospheric and chromospheric heights, respectively, then we obtain a lag time of about 180 ± 12 s. If we assume that the height between the TiO and H_α channels is about 1500 ± 250 km (Avrett & Loeser 2008), then the phase speed for the propagating wave is about 8.9 ± 0.18 km s⁻¹ for the five minute band. For the three minute band, we obtained a propagation speed at 8.3 ± 0.18 km s⁻¹.

For a propagation slow mode wave, the oscillation period is found at three minute and five minute bands. The propagation speed is about 8–9 km s⁻¹, so the local temperature is about 2800–3500 K. This temperature is smaller

than temperature minimum of an empirical sunspot model (Avrett & Loeser 2008). However, we should note this is lower limit estimations because we did not consider the projection effect. This study could also be used as an effective tool to probe the temperature of a sunspot.

Acknowledgements The authors gratefully acknowledge the anonymous referee for his/her critical reading and invaluable comments and suggestions. Song Feng is supported by the Joint Funds of the National Natural Science Foundation of China (NSFC, U1931107) and the Key Applied Basic Research Program of Yunnan Province (2018FA035). Ding Yuan is supported by the NSFC (Nos. 11803005 and 11911530690) and Shenzhen Technology Project (JCYJ20180306172239618). Xiao Yang is supported by the NSFC (Grant Nos. 11427901, 11673038, 11773038, 11873062 and 11973056). We thank the Open Research Program (KLSA202007) of Key Laboratory of Solar Activity of National Astronomical Observatory of China. We thank the NVST team for their high-resolution observations.

Appendix A: VARIATIONS OF THE UMBRA AREAS AND EMISSION INTENSITIES OBSERVED BY SDO/AIA

The variations of the umbra areas and the umbra intensities are taken from the SDO/AIA 1700 Å channel and shown in Fig. A.1. The SST spectra of the areas and the intensities are plotted in Fig. A.2. The in-phase behavior can easily be found from Fig. A.2.

References

- Avrett, E. H., & Loeser, R. 2008, *The Astrophysical Journal Supplement Series*, 175, 229
- Bai, X. Y., Deng, Y. Y., & Su, J. T. 2013, *Solar Physics*, 282, 405
- Bai, X. Y., Deng, Y. Y., Teng, F., et al. 2014, *MNRAS*, 445, 49
- Chen, S.-X., Li, B., Shi, M., & Yu, H. 2018, *ApJ*, 868, 5
- Chen, S.-X., Li, B., Xia, L.-D., & Yu, H. 2015, *Solar Physics*, 290, 2231
- Daubechies, I., Lu, J., & Wu, H.-T. 2011, *Applied and Computational Harmonic Analysis*, 30, 243
- Dorotovic, I., Erdélyi, R., Freij, N., et al. 2014, *A&A*, 563, A12
- Edwin, P. M., & Roberts, B. 1983, *Sol. Phys.*, 88, 179
- Feng, S., Deng, L., Shu, G., et al. 2012, in *IEEE Fifth International Conference on Advanced Computational Intelligence*, (New York: IEEE Press), 626
- Freij, N., Dorotovic, I., Morton, R. J., et al. 2016, *ApJ*, 817, 44
- Goossens, M., Van Doorsselaere, T., Soler, R., et al. 2013, *ApJ*, 768, 191
- Grant, S. D. T., Jess, D. B., Moreels, M. G., et al. 2015, *ApJ*, 806, 132

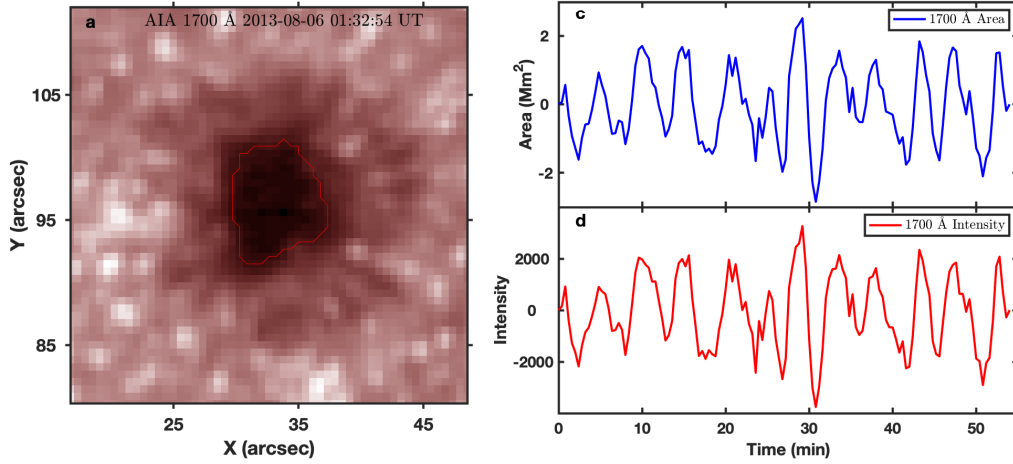


Fig. A.1 Same as Figs. 1 and 2 but with the AIA 1700 Å data set.

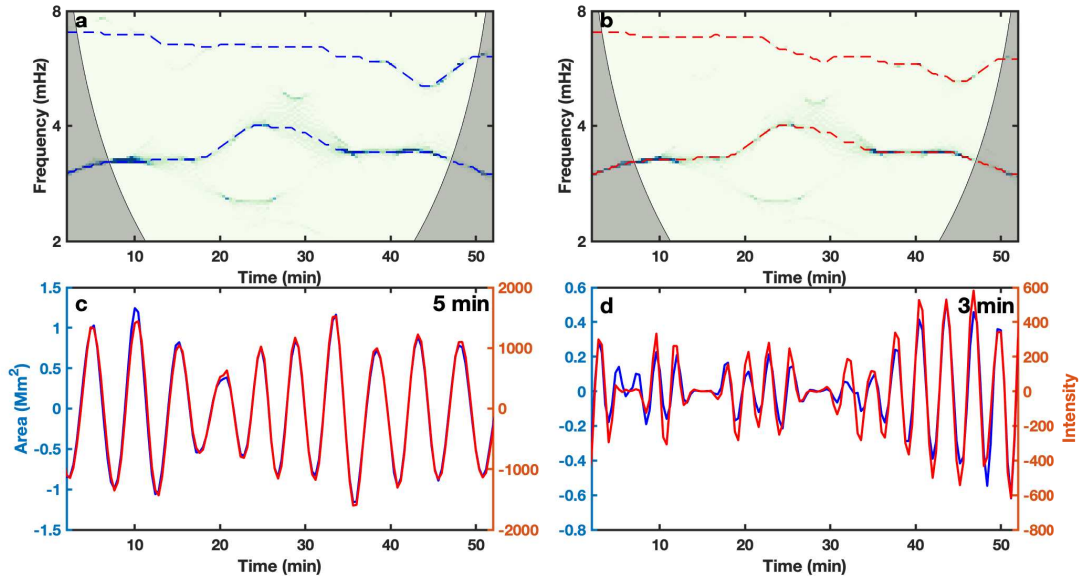


Fig. A.2 Same as Fig. 3 but with the AIA 1700 Å data set.

Huang, N. E., Shen, Z., Long, S. R., et al. 1998, in Royal Society of London Proceedings Series A, NASA Goddard Space Flight Center, 903
 Inglis, A. R., Van Doorselaere, T., Brady, C. S., et al. 2009, *A&A*, 503, 569
 Jess, D. B., Reznikova, V. E., Van Doorselaere, T., et al. 2013, *ApJ*, 779, 168
 Keys, P. H., Morton, R. J., Jess, D. B., et al. 2018, *ApJ*, 857, 28
 Li, B., Chen, S.-X., Xia, L.-D., & Yu, H. 2014, *A&A*, 568, A31
 Liu, Z., Xu, J., Gu, B.-Z., et al. 2014, *RAA (Research in Astronomy and Astrophysics)*, 14, 705
 McLaughlin, J. A., Nakariakov, V. M., Dominique, M., et al. 2018, *Space Sci. Rev.*, 214, 45
 Moreels, M. G., Freij, N., Erdélyi, R., et al. 2015, *A&A*, 579, A73
 Moreels, M. G., Goossens, M., & Van Doorselaere, T. 2013, *A&A*, 555, A75

Nakariakov, V. M., Hornsey, C., & Melnikov, V. F. 2012, *ApJ*, 761, 134
 Nakariakov, V. M., & Melnikov, V. F. 2009, *Space Sci. Rev.*, 149, 119
 Shi, M., Li, B., Huang, Z., & Chen, S.-X. 2019, *ApJ*, 874, 87
 Su, J. T., Ji, K. F., Banerjee, D., et al. 2016, *ApJ*, 816, 30
 Tian, H., Young, P. R., Reeves, K. K., et al. 2016, *ApJ*, 823, L16
 Vasheghani Farahani, S., Hornsey, C., Van Doorselaere, T., et al. 2014, *ApJ*, 781, 92
 Wang, Z.-K., Feng, S., Deng, L.-H., et al. 2020, *RAA (Research in Astronomy and Astrophysics)*, 20, 006
 Yu, H., Li, B., Chen, S.-X., et al. 2016, *ApJ*, 833, 51
 Yuan, D., Su, J., Jiao, F., et al. 2016, *ApJS*, 224, 30
 Yuan, D., Van Doorselaere, T., Banerjee, D., et al. 2015, *ApJ*, 807, 98
 Yuan, D., & Walsh, R. W. 2016, *A&A*, 594, A101